Received: 14 May 2024 | Accepted: 3 June 2024

DOI: 10.1002/pip.3831

SHORT COMMUNICATION

PROGRESS IN PHOTOVOLTAICS WILEY

Solar cell efficiency tables (Version 64)

Martin A. Green[1] | Ewan D. Dunlop[2] | Masahiro Yoshita[3] | Nikos Kopidakis[4] | Karsten Bothe[5] | Gerald Siefer[6] | David Hinken[5] | Michael Rauer[6] | Jochen Hohl-Ebinger[6] | Xiaojing Hao[1]

[1]Australian Centre for Advanced Photovoltaics, School of Photovoltaic and Renewable Energy Engineering, University of New South Wales, Sydney, 2052, Australia

[2]European Commission–Joint Research Centre, Ispra, (VA), Italy

[3]Renewable Energy Research Center (RENRC), National Institute of Advanced Industrial Science and Technology (AIST), Central 2, Umezono 1-1-1, Tsukuba, Ibaraki, 305-8568, Japan

[4]National Renewable Energy Laboratory, 15013 Denver West Parkway, Golden, Colorado, 80401, USA

[5]Calibration and Test Center (CalTeC), Solar Cells Laboratory, Institut für Solarenergieforschung GmbH (ISFH), Am Ohrberg 1, Emmerthal, D-31860, Germany

[6]Fraunhofer-Institute for Solar Energy Systems–ISE CalLab, Heidenhofstr. 2, Freiburg, D-79110, Germany

Correspondence
Martin A. Green, Australian Centre for Advanced Photovoltaics, School of Photovoltaic and Renewable Energy Engineering, University of New South Wales, Sydney 2052, Australia.
Email: m.green@unsw.edu.au

Funding information
Australian Renewable Energy Agency, Grant/Award Number: SRI-001; U.S. Department of Energy (Office of Science, Office of Basic Energy Sciences and Energy Efficiency and Renewable Energy, Solar Energy Technology Program), Grant/Award Number: DE-AC36-08-GO28308; Ministry of Economy, Trade and Industry

Abstract

Consolidated tables showing an extensive listing of the highest independently confirmed efficiencies for solar cells and modules are presented. Guidelines for inclusion of results into these tables are outlined, and new entries since January 2024 are reviewed.

KEYWORDS

energy conversion efficiency, photovoltaic efficiency, solar cell efficiency

1 | INTRODUCTION

Since January 1993, '*Progress in Photovoltaics*' has published six monthly listings of the highest confirmed efficiencies for a range of photovoltaic cell and module technologies.[1–3] By providing guidelines for inclusion of results into these tables, this not only provides an authoritative summary of the current state-of-the-art but also encourages researchers to seek independent confirmation of results and to report results on a standardised basis. In Version 33 of these tables, results were updated to the new internationally accepted reference spectrum (International Electrotechnical Commission IEC 60904-3, Ed. 2, 2008).

The most important criterion for inclusion of results into the tables is that they must have been independently measured by a recognised test centre listed in Versions 61 and 62. A distinction is made between three different eligible definitions of cell area: total area, aperture area and designated illumination area, as also defined elsewhere[2] (note that, if masking is used, masks must have a simple aperture geometry, such as square, rectangular or circular—masks with multiple openings are not eligible). 'Active area' efficiencies are not included. There are also certain minimum values of the area sought for the different device types (above 0.05 cm^2 for a concentrator cell, 1 cm^2 for a one-sun cell, 200 cm^2 for a 'submodule' and 800 cm^2 for a module).

TABLE 1 Confirmed single-junction terrestrial cell and submodule efficiencies measured under the global AM1.5 spectrum (1000 W/m^2) at 25°C (IEC 60904-3: 2008 or ASTM G-173-03 global).

Classification	Efficiency (%)	Area (cm^2)	V_{oc} (V)	J_{sc} (mA/cm^2)	Fill factor (%)	Test centre (date)	Description
Silicon							
Si (crystalline cell)	**27.3 ± 0.4[a]**	**243.1 (da)**	**0.7434**	**42.60[b]**	**86.2**	**ISFH (12/23)**	**LONGi, n-type HBC[4]**
Si (thin transfer submodule)	21.2 ± 0.4	239.7 (ap)	0.687[c]	38.50[c,d]	80.3	NREL (4/14)	Solexel (35 μm thick)[5]
Si (thin film minimodule)	10.5 ± 0.3	94.0 (ap)	0.492[c]	29.7[c,e]	72.1	FhG-ISE (8/07)	CSG Solar (<2 μm on glass)[6]
III-V cells							
GaAs (thin film cell)	29.1 ± 0.6	0.998 (ap)	1.1272	29.78[f]	86.7	FhG-ISE (10/18)	Alta Devices[7]
GaAs (multicrystalline)	18.4 ± 0.5	4.011 (t)	0.994	23.2	79.7	NREL (11/95)	RTI, Ge substrate[8]
InP (crystalline cell)	24.2 ± 0.5[g]	1.008 (ap)	0.939	31.15[h]	82.6	NREL (3/13)	NREL[9]
Thin film chalcogenide							
CIGS (cell) (Cd-free)	23.35 ± 0.5	1.043 (da)	0.734	39.58[i]	80.4	AIST (11/18)	Solar Frontier[10]
CIGSSe (submodule)	20.3 ± 0.4	526.7 (ap)	0.6834	39.55[c,j]	75.1	NREL (5/23)	Avancis, 100 cells[11]
CdTe (cell)	21.0 ± 0.4	1.0623 (ap)	0.8759	30.25[d]	79.4	Newport (8/14)	First Solar, on glass[12]
CZTSSe (cell)	**13.45 ± 0.3**	**1.101 (da)**	**0.5109**	**37.90[b]**	**69.5**	**NPVM (4/24)**	**IoP/CAS[13]**
CZTSSe (minimodule)	**10.1 ± 0.3**	**10.48 (da)**	**0.5309[c]**	**32.77[c,b]**	**57.9**	**NREL (1/24)**	**NJUPT, 6 serial cells[14]**
CZTS (cell)	10.0 ± 0.2	1.113 (da)	0.7083	21.77[h]	65.1	NREL (3/17)	UNSW[15]
Amorphous/Microcrystalline							
Si (amorphous cell)	10.2 ± 0.3[g,k]	1.001 (da)	0.896	16.36[d]	69.8	AIST (7/14)	AIST[16]
Si (microcrystalline cell)	11.9 ± 0.3[g]	1.044 (da)	0.550	29.72[h]	75.0	AIST (2/17)	AIST[17]
Perovskite							
Perovskite (cell)	25.2 ± 0.8[l]	1.0347 (da)	1.162	26.39[j]	82.0	Newport (7/23)	NorthwesternU[18]
Perovskite (minimodule)	**22.6 ± 0.5[l]**	**20.25 (da)**	**1.169[c]**	**25.00[c,b]**	**77.4**	**NPVM (5/24)**	**Singfilm, 8 cells[19]**
Dye sensitised							
Dye (cell)	11.9 ± 0.4[m]	1.005 (da)	0.744	22.47[n]	71.2	AIST (9/12)	Sharp[20,21]
Dye (minimodule)	10.7 ± 0.4[m]	26.55 (da)	0.754[c]	20.19[c,o]	69.9	AIST (2/15)	Sharp, 7 serial cells[20,21]
Dye (submodule)	8.8 ± 0.3[m]	398.8 (da)	0.697[c]	18.42[c,p]	68.7	AIST (9/12)	Sharp, 26 serial cells[20,21]
Organic							
Organic (cell)	**15.8 ± 0.3[g,q]**	**1.064 (da)**	**0.8513**	**25.11[b]**	**73.9**	**FhG-ISE (6/23)**	**Fraunhofer ISE/FMF[22]**
Organic (minimodule)	15.7 ± 0.3[q]	19.31(da)	0.8771[c]	24.37[c,j]	73.4	JET (1/23)	ZhejiangU, 7 cells[23]
Organic (submodule)	**14.5 ± 0.2[q]**	**204.11 (da)**	**0.8315[c]**	**23.32[c,b]**	**74.6**	**FhG-ISE (11/23)**	**FAU/FZJ, 38 cells[24]**

Abbreviations: CIGS, $CuIn_{1-y}Ga_ySe_2$; a-Si, amorphous silicon/hydrogen alloy; nc-Si, nanocrystalline or microcrystalline silicon; CZTSSe, $Cu_2ZnSnS_{4-y}Se_y$; CZTS, Cu_2ZnSnS_4; (ap), aperture area; (t), total area; (da), designated illumination area; ISFH, Institute für Solarenergieforschung; NREL, US National Renewable Energy Laboratory; FhG-ISE, Fraunhofer Institut für Solare Energiesysteme; AIST, Japanese National Institute of Advanced Industrial Science and Technology; NPVM, Chinese National Photovoltaic Industry Measurement and Testing Center; JET, Japan Electrical Safety and Environment Technology Laboratories.

[a]Contacting: Front: Unmetallised; Rear: Rear: 2 × 6BB, busbar resistance neglecting (brn) contacting, highly reflective (white) chuck (hrc).
[b]Spectral response and current–voltage curve reported in the present version of these tables.
[c]Reported on a 'per cell' basis.
[d]Spectral responses and current–voltage curve reported in Version 45 of these tables.
[e]Recalibrated from original measurement.
[f]Spectral response and current–voltage curve reported in Version 53 of these tables.
[g]Not measured at an external laboratory.
[h]Spectral response and current–voltage curve reported in Version 50 of these tables.
[i]Spectral response and current–voltage curve reported in Version 54 of these tables.
[j]Spectral response and current–voltage curve reported in Version 62 of these tables.
[k]Stabilised by 1000-h exposure to 1 sun light at 50°C.
[l]Initial performance. Boyd et al.[25] and You[26] review the stability of similar devices.
[m]Initial efficiency. Krašovec et al.[27] reviews the stability of similar devices.
[n]Spectral response and current–voltage curve reported in Version 41 of these tables.
[o]Spectral response and current–voltage curve reported in Version 46 of these tables.
[p]Spectral response and current–voltage curve reported in Version 43 of these tables.
[q]Initial performance. Tanenbaum et al.[28] and Krebs[29] review the stability of similar devices.

In recent years, approaches for contacting large-area solar cells during measurement have become increasingly complex. Since there is no explicit standard for the design of solar cell contacting units, in an earlier issue,[3] we describe approaches for temporary electrical contacting of large-area solar cells both with and without busbars. To enable comparability between different contacting approaches and to clarify the corresponding measurement conditions, an unambiguous denotation was introduced and used in subsequent versions of these tables. Since efficiency, particularly fill factor, appears to be overestimated in many recent results reported outside these tables (especially for unencapsulated, large area cells with poorly conducting busbars, prior to soldering interconnection ribbons or wires)—due to incorrect probing (this applies even to cells independently measured)—we include an appendix in the present issue that describes the best probing approaches.

Tabled results are reported for cells and modules made from different semiconductors and for sub-categories within each

TABLE 2 'Notable Exceptions' for single-junction cells and submodules: 'Top dozen' confirmed results, not class records, measured under the global AM1.5 spectrum (1000 Wm^{-2}) at 25°C (IEC 60904-3: 2008 or ASTM G-173-03 global).

Classification	Efficiency (%)	Area (cm^2)	V_{oc} (V)	J_{sc} (mA/cm^2)	Fill factor (%)	Test centre (date)	Description
Cells (silicon)							
Si	25.0 ± 0.5	4.00 (da)	0.706	42.7[a]	82.8	Sandia (3/99)	UNSW, p-type PERC[30]
Si	25.8 ± 0.5[b]	4.008 (da)	0.7241	42.87[c]	83.1	FhG-ISE (7/17)	FhG-ISE, n-type TOPCon[31]
Si	26.0 ± 0.5[b]	4.015 (da)	0.7323	42.05[d]	84.3	FhG-ISE (11/19)	FhG-ISE, p-type TOPCon
Si	26.1 ± 0.3[b]	3.9857 (da)	0.7266	42.62[e]	84.3	ISFH (2/18)	ISFH, p-type TBC[32]
Si (large)	24.0 ± 0.3[f]	244.59 (t)	0.6940	41.58[g]	83.3	ISFH (7/19)	LONGi, p-type PERC[33]
Si (large)	**25.6 ± 0.4**[h]	**330.3 (t)**	**0.7418**	**41.39**[i]	**83.5**	**ISFH (3/24)**	**JASolar, n-type TOPCon**[34]
Si (large)	**26.8 ± 0.4**	**274.4 (t)**	**0.7514**	**41.45**[i]	**86.1**	**ISFH (10/22)**	**LONGi, n-type HJT**[35]
Si (large)	26.6 ± 0.4[j]	274.1 (t)	0.7513	41.30	85.6	ISFH (10/22)	LONGi, p-type HJT[36]
Cells (III-V)							
GaInP	22.0 ± 0.3[b]	0.2502 (ap)	1.4695	16.63[l]	90.2	NREL (1/19)	NREL, rear HJ, strained AlInP[37]
Cells (chalcogenide)							
CIGS (thin-film)	23.6 ± 0.4	0.899 (da)	0.7671	38.30[m]	80.5	FhG-ISE (1/23)	Evolar/UppsalaU[38]
CdTe (thin-film)	**22.6 ± 0.3**	**0.4486 (da)**	**0.8981**	**31.56**[i]	**79.6**	**NREL (1/24)**	**First Solar**[39]
CZTSSe (thin-film)	**15.1 ± 0.3**	**0.2697 (da)**	**0.5299**	**38.44**[i]	**74.0**	**NPVM (4/24)**	**IoP/CAS**[13]
CZTS (thin-film; >1.5 eV)	**12.1 ± 0.3**	**0.2021(da)**	**0.7490**	**23.40**[i]	**68.9**	**NPVM (5/24)**	**UNSW**[40]
S							
Perovskite (thin-film)	**26.7 ± 0.6**[n,o]	**0.0519 (da)**	**1.193**	**26.49**[i]	**84.5**	**NPVM (5/24)**	**USTC**[41]
Organic (thin-film)	19.2 ± 0.3[p]	0.0326 (da)	0.9135	26.61[m]	79.0	NREL (3/23)	SJTU[42]
Dye sensitised	13.0 ± 0.4[q]	0.1155 (da)	1.0396	15.55[m]	80.4	FhG-ISE (10/20)	EPFL[43]

Abbreviations: CIGS, $CuIn_{1-y}Ga_ySe_2$; CZTSSe, $Cu_2ZnSnS_{4-y}Se_y$; CZTS, Cu_2ZnSnS_4; (ap), aperture area; (t), total area; (da), designated illumination area; AIST, Japanese National Institute of Advanced Industrial Science and Technology; NREL, National Renewable Energy Laboratory; FhG-ISE, Fraunhofer-Institut für Solare Energiesysteme; ISFH, Institute for Solar Energy Research, Hamelin.

[a]Spectral response reported in Version 36 of these tables.

[b]Not measured at an external laboratory.

[c]Spectral response and current–voltage curves reported in Version 51 of these tables.

[d]Spectral response and current–voltage curves reported in Version 55 of these tables.

[e]Spectral response and current–voltage curve reported in Version 52 of these tables.

[f]Contacting: Front: 12BB, resistance neglecting (brn); Rear: fully metallized, full area contacting (fac).

[g]Spectral response and current–voltage curves reported in Version 57 of these tables.

[h]Contacting: 16BB, busbar resistance neglecting (brn); Rear: 16BB, grid resistance neglecting (grn) contacting, highly reflective (gold) chuck (hrc).

[i]Spectral response and current–voltage curves reported in the present version of these tables.

[j]Contacting: Front: 12BB, busbar resistance neglecting (brn) contacting; Rear: 12BB, grid resistance neglecting (grn) contacting, highly reflective (gold) chuck (hrc).

[k]Spectral response and current–voltage curves reported in Version 50 of these tables.

[l]Spectral response and current–voltage curve reported in Version 54 of these tables.

[m]Spectral response and current–voltage curves reported in Version 62 of these tables.

[n]Stability not investigated. Boyd et al.[25] and Yang and You[26] document the stability of similar devices.

[o]Measured using a 10-point IV sweep with constant voltage bias until a current change rate of <0.07%/min.

[p]Long-term stability not investigated. Tanenbaum et al.[28] and Krebs[29] document the stability of similar devices.

[q]Long-term stability not investigated. Krašovec et al.[27] document the stability of similar devices.

TABLE 3 Confirmed multiple-junction terrestrial cell and submodule efficiencies measured under the global AM1.5 spectrum (1000 W/m^2) at 25°C (IEC 60904-3: 2008 or ASTM G-173-03 global).

Classification	Efficiency (%)	Area (cm^2)	V_{oc} (V)	J_{sc} (mA/cm^2)	Fill factor (%)	Test centre (date)	Description
III-V Multijunctions							
5 junction cell (bonded) (2.17/1.68/1.40/1.06/.73 eV)	38.8 ± 1.2	1.021 (ap)	4.767	9.564	85.2	NREL (7/13)	Spectrolab, 2-terminal
InGaP/GaAs/InGaAs	37.9 ± 1.2	1.047 (ap)	3.065	14.27[a]	86.7	AIST (2/13)	Sharp, 2 term.[44]
GaInP/GaAs (monolithic)	32.8 ± 1.4	1.000 (ap)	2.568	14.56[b]	87.7	NREL (9/17)	LG Electronics, 2 term.
III-V/Si Multijunctions							
GaInP/GaInAsP//Si (bonded)	36.1 ± 1.3[c]	3.987 (ap)	3.309	12.70[d]	86.0	FhG-ISE (5/23)	FhG-ISE/AMOLF, 2-term.[45]
GaInP/GaAs/Si (mech. stack)	35.9 ± 0.5[c]	1.002 (da)	2.52/0.681	13.6/11.0	87.5/78.5	NREL (2/17)	NREL/CSEM/EPFL, 4-term.[46]
GaInP/GaAs/Si (monolithic)	25.9 ± 0.9[c]	3.987 (ap)	2.647	12.21[e]	80.2	FhG-ISE (6/20)	Fraunhofer ISE, 2-term.[47]
GaAsP/Si (monolithic)	23.4 ± 0.3	1.026 (ap)	1.732	17.34[f]	77.7	NREL (5/20)	OSU/UNSW/SolAero, 2-term[48]
GaAs/Si (mech. stack)	32.8 ± 0.5[c]	1.003 (da)	1.09/0.683	28.9/11.1[g]	85.0/79.2	NREL (12/16)	NREL/CSEM/EPFL, 4-term.[46]
GaInP/GaInAs/Ge; Si (spectral split minimodule)	34.5 ± 2.0	27.83 (ap)	2.66/0.65	13.1/9.3	85.6/79.0	NREL (4/16)	UNSW/Azur/Trina, 4-term.[49]
Perov./Si Multijunctions							
Perovskite/Si	**34.2 ± 1.0[h]**	**1.0044(da)**	**1.990**	**20.65[i]**	**83.2**	**ESTI (4/24)**	**LONGi, 2-term.**
Perovskite/Si (large)	28.6 ± 1.4[h]	258.14(t)	1.909	19.11[j]	78.3	FhG-ISE (5/23)	Oxford PV, 2-term.[50]
Other Multijunctions							
Perovskite/CIGS	24.2 ± 0.7[h]	1.045 (da)	1.768	19.24[f]	72.9	FhG-ISE (1/20)	HZB, 2-terminal[59]
Perovskite/perovskite	28.2 ± 0.5[h]	1.038(da)	2.159	16.59[j]	78.9	JET (12/22)	NanjingU/Renshine, 2-term.[51]
Perovskite/perovskite (minimodule)	24.5 ± 0.6[h]	20.25(da)	2.157	14.86[k]	77.5	JET (6/22)	NanjingU/Renshine, 2-term.[53]
a-Si/nc-Si/nc-Si (thin-film)	14.0 ± 0.4[c,l]	1.045 (da)	1.922	9.94[m]	73.4	AIST (5/16)	AIST, 2-term.[53]
a-Si/nc-Si (thin-film cell)	12.7 ± 0.4[c,l]	1.000(da)	1.342	13.45[n]	70.2	AIST (10/14)	AIST, 2-term.[54]
'Notable Exceptions'							
GaInP/GaAs (mqw)	32.9 ± 0.5[c]	0.250 (ap)	2.500	15.36[o]	85.7	NREL (1/20)	NREL/UNSW, multiple QW
GaInP/GaAs/GaInAs	37.8 ± 1.4	0.998 (ap)	3.013	14.60[o]	85.8	NREL (1/18)	Microlink (ELO)[56]
GaInP/GaAs (mqw)/GaInAs	39.5 ± 0.5[c]	0.242 (ap)	2.997	15.44[p]	85.3	NREL (9/21)	NREL, multiple QW
6 junction (monolithic) (2.19/1.76/1.45/1.19/.97/.7 eV)	39.2 ± 3.2[c]	0.247 (ap)	5.549	8.457[q]	83.5	NREL (11/18)	NREL, inv. metamorphic[56]
GaInP/AlGaAs/CIGS	28.1 ± 1.2[c]	0.1386(da)	2.952	11.72[r]	81.1	AIST (1/21)	AIST/FhG-ISE, 2-term.[57]
Perovskite/perovskite	**30.1 ± 0.8[h]**	**0.0493(da)**	**2.20**	**16.72[i]**	**81.8**	**JET (10/23)**	**NanjingU/Renshine, 2-term.[52]**
Perovskite/organic	23.4 ± 0.8[h]	0.0552(da)	2.136	14.56[s]	75.6	JET (3/22)	NUS/SERIS, 2-term.[58]

Abbreviations: a-Si, amorphous silicon/hydrogen alloy; nc-Si, nanocrystalline or microcrystalline silicon; (ap), aperture area; (t), total area; (da), designated illumination area; NREL, US National Renewable Energy Laboratory; AIST, Japanese National Institute of Advanced Industrial Science and Technology; FhG-ISE, Fraunhofer Institut für Solare Energiesysteme; ESTI, European Solar Test Installation; JET, Japan Electrical Safety and Environment Technology Laboratories.

[a]Spectral response and current–voltage curve reported in Version 42 of these tables.

[b]Spectral response and current–voltage curve reported in the Version 51 of these tables.
[c]Not measured at an external laboratory.
[d]Spectral response and current–voltage curves reported in the present version of these tables.
[e]Spectral response and current–voltage curve reported in Version 57 of these tables.
[f]Spectral response and current–voltage curve reported in Version 56 of these tables.
[g]Spectral response and current–voltage curve reported in Version 52 of these tables.
[h]Initial efficiency. Boyd et al.[25] and Yang and You[26] review the stability of similar perovskite-based devices.
[i]Spectral response and current–voltage curves reported in the present version of these tables.
[j]Spectral response and current–voltage curve reported in Version 63 of these tables.
[k]Spectral response and current–voltage curve reported in Version 61 of these tables.
[l]Stabilised by 1000-h exposure to 1 sun light at 50°C.
[m]Spectral response and current–voltage curve reported in Version 49 of these tables.
[n]Spectral responses and current–voltage curve reported in Version 45 of these tables.
[o]Spectral response and current–voltage curve reported in Version 53 of these tables.
[p]Spectral response and current–voltage curves reported in Version 59 of these tables.
[q]Spectral response and current–voltage curve reported in Version 54 of these tables.
[r]Spectral response and current–voltage curve reported in Version 58 of these tables.
[s]Spectral response and current–voltage curve reported in Version 60 of these tables.

TABLE 4 Confirmed non-concentrating terrestrial module efficiencies measured under the global AM1.5 spectrum (1000 W/m^2) at a cell temperature of 25°C (IEC 60904-3: 2008 or ASTM G-173-03 global).

Classification	Effic.(%)	Area (cm^2)	V_{oc} (V)	I_{sc} (A)	FF (%)	Test Centre (date)	Description
Si (crystalline)	**24.9 ± 0.3**	**17,753 (da)**	**83.08**	**6.413[a]**	**82.8**	**NREL (1/24)**	**Maxeon (112 cells)[60]**
GaAs (thin-film)	25.1 ± 0.8	866.45 (ap)	11.08	2.303[b]	85.3	FhG-ISE (11/17)	Alta Devices[61]
CIGS (Cd-free)	19.2 ± 0.5	841 (ap)	48.0	0.456[c]	73.7	AIST (1/17)	Solar Frontier (70 cells)[62]
CdTe (thin-film)	**19.9 ± 0.3**	**23,932 (da)**	**231.5**	**2.675[a]**	**77.1**	**NREL (6/23)**	**First Solar[63]**
Perovskite	**19.2 ± 0.4[d]**	**1027 (da)**	**59.4**	**0.4307[a]**	**77.1**	**NREL (12/23)**	**SolaEon[64]**
Organic	13.1 ± 0.3[e]	1475 (da)	48.10	0.6015[f]	67.0	NREL (5/23)	Waystech/Nanobit[65]
Multijunction							
InGaP/GaAs/InGaAs	32.65 ± 0.7	965 (da)	24.30	1.520[g]	85.3	AIST (2/22)	Sharp (40 cells; 8 series)[66]
Perovskite/Si	**25.8 ± 2.1[d]**	**2054 (da)**	**110/8.75**	**0.40/2.83[a]**	**75.4/81.8**	**FhG-ISE (4/24)**	**LONGi, 4-terminal[67]**
a-Si/nc-Si (tandem)	12.3 ± 0.3[h]	14,322 (t)	280.1	0.902[i]	69.9	ESTI (9/14)	TEL Solar, Trubbach Labs[68]
'Notable Exceptions'							
CIGS (large)	18.6 ± 0.6	10,858 (ap)	58.00	4.545[j]	76.8	FhG-ISE (10/19)	Miasole[69]
InGaP/GaAs//Si	33.7 ± 0.7	775 (da)	20.3/2.83	1.25/1.93[f]	86.5/78.0	AIST (2/23)	Sharp/Toyota TI, 4-term.[70]
InGaP/GaAs//CIGS	31.2 ± 0.7	778 (ap)	20.3/16.9	1.24/.26[f]	85.7/59.8	AIST (2/23)	Sharp/Idemitsu, 4-term.[70]
Perovskite (large)	**15.0 ± 0.5[d]**	**7906 (da)**	**206.05**	**0.752[a]**	**76.5**	**FhG-ISE (1/24)**	**Microquanta[71]**

Abbreviations: CIGSS, CuInGaSSe; a-Si, amorphous silicon/hydrogen alloy; a-SiGe, amorphous silicon/germanium/hydrogen alloy; nc-Si, nanocrystalline or microcrystalline silicon; Effic., efficiency; (t), total area; (ap), aperture area; (da), designated illumination area; FF, fill factor.
[a]Spectral response and current–voltage curve reported in the present version of these tables.
[b]Spectral response and current–voltage curve reported in Version 51 of these tables.
[c]Spectral response and current–voltage curve reported in Version 50 of these tables.
[d]Initial performance. Boyd et al.[25] and Yang and You[26] review the stability of similar devices.
[e]Initial performance. Tanenbaum et al.[28] and Krebs[29] review the stability of similar devices.
[f]Spectral response and current voltage curve reported Version 62 of these tables.
[g]Spectral response and current–voltage curve reported in Version 60 of these tables.
[h]Stabilised at the manufacturer to the 2% level following IEC procedure of repeated measurements.
[i]Spectral response and/or current–voltage curve reported in Version 46 of these tables.
[j]Spectral response and current–voltage curve reported in Version 55 of these tables.

semiconductor grouping. From Version 36 onwards, spectral response information is included (when possible) in the form of a plot of the external quantum efficiency (EQE) versus wavelength, either as absolute values or normalised to the peak measured value. Current–voltage (IV) curves have also been included where possible from Version 38 onwards.

Highest confirmed 'one sun' cell and module results are reported in Tables 1–4. Any changes in the tables from those

TABLE 5 Terrestrial concentrator cell and module efficiencies measured under the ASTM G-173-03 direct beam AM1.5 spectrum at a cell temperature of 25°C (except where noted for the hybrid and luminescent modules).

Classification	Effic. (%)	Area (cm^2)	Intensity[a] (suns)	Test Centre (date)	Description
Single Cells					
GaAs	30.8 ± 1.9[b,c]	0.0990 (da)	61	NREL (1/22)	NREL, 1 junction (1 J)
Si	27.6 ± 1.2[d]	1.00 (da)	92	FhG-ISE (11/04)	Amonix back-contact[72]
CIGS (thin-film)	23.3 ± 1.2[b,e]	0.09902 (ap)	15	NREL (3/14)	NREL[73]
Multijunction cells					
AlGaInP/AlGaAs/GaAs/GaInAs(3) (2.15/1.72/1.41/1.17/0.96/0.70 eV)	47.1 ± 2.6[b,f]	0.099 (da)	143	NREL (3/19)	NREL, 6 J inv. metamorphic[56]
GaInP/GaInAs; GaInAsP/GaInAs	47.6 ± 2.6[b,g]	0.0452 (da)	665	FhG-ISE (5/22)	FhG-ISE 4 J bonded[74]
GaInP/GaAs/GaInAs/GaInAs	45.7 ± 2.3[b,h]	0.09709 (da)	234	NREL (9/14)	NREL, 4 J monolithic[75]
InGaP/GaAs/InGaAs	44.4 ± 2.6[i]	0.1652 (da)	302	FhG-ISE (4/13)	Sharp, 3 J inverted metamorphic[76]
GaInAsP/GaInAs	35.5 ± 1.2[b,j]	0.10031 (da)	38	NREL (10/17)	NREL 2-junction (2 J)[77]
Minimodule					
GaInP/GaAs; GaInAsP/GaInAs	43.4 ± 2.4[b,k]	18.2 (ap)	340[l]	FhG-ISE (7/15)	Fraunhofer ISE 4 J (lens/cell)[78]
Submodule					
GaInP/GaInAs/Ge; Si	40.6 ± 2.0[k]	287 (ap)	365	NREL (4/16)	UNSW 4 J split spectrum[79]
Modules					
Si	20.5 ± 0.8[b]	1875 (ap)	79	Sandia (4/89)[l]	Sandia/UNSW/ENTECH (12 cells)[80]
Three Junction (3 J)	35.9 ± 1.8[m]	1092 (ap)	N/A	NREL (8/13)	Amonix[81]
Four Junction (4 J)	38.9 ± 2.5[n]	812.3 (ap)	333	FhG-ISE (4/15)	Soitec[82]
Hybrid Module[o]					
4-Junction (4 J)/bifacial c-Si	34.2 ± 1.9[b,o]	1088 (ap)	CPV/PV	FhG-ISE (9/19)	FhG-ISE (48/8 cells; 4 T)[83]
'Notable Exceptions'					
Si (large area)	21.7 ± 0.7	20.0 (da)	11	Sandia (9/90)[l]	UNSW laser grooved[84]
Luminescent Minimodule[o]	7.1 ± 0.2	25 (ap)	2.5[p]	ESTI (9/08)	ECN Petten, GaAs cells[85]
4J Minimodule	41.4 ± 2.6[b]	121.8 (ap)	230	FhG-ISE (9/18)	FhG-ISE, 10 cells[86]

Note: Following the normal convention, efficiencies calculated under this direct beam spectrum neglect the diffuse sunlight component that would accompany this direct spectrum. These direct beam efficiencies need to be multiplied by a factor estimated as 0.8746 to convert to thermodynamic efficiencies.[87]

Abbreviations: CIGS, $CuInGaSe_2$; Effic., efficiency; (da), designated illumination area; (ap), aperture area; NREL, National Renewable Energy Laboratory; FhG-ISE, Fraunhofer-Institut für Solare Energiesysteme; ESTI, European Solar Test Installation.

[a]One sun corresponds to direct irradiance of 1000 Wm^{-2}.

[b]Not measured at an external laboratory.

[c]Spectral response and current–voltage curve reported in Version 60 of these tables.

[d]Measured under a low aerosol optical depth spectrum similar to ASTM G-173-03 direct.[88]

[e]Spectral response and current–voltage curve reported in Version 44 of these tables.

[f]Spectral response and current–voltage curve reported in Version 54 of these tables.

[g]Spectral response and current–voltage curve reported in Version 61 of these tables.

[h]Spectral response and current–voltage curve reported in Version 46 of these tables.

[i]Spectral response and current–voltage curve reported in Version 42 of these tables.

[j]Spectral response and current–voltage curve reported in Version 51 of these tables.

[k]Determined at IEC 62670-1 CSTC reference conditions.

[l]Recalibrated from original measurement.

[m]Referenced to 1000-W/m^2 direct irradiance and 25°C cell temperature using the prevailing solar spectrum and an in-house procedure for temperature translation.

[n]Measured under IEC 62670-1 reference conditions following the current IEC power rating draft 62670-3.

[o]Thermodynamic efficiency. Hybrid and luminescent modules measured under the ASTM G-173-03 or IEC 60904-3: 2008 global AM1.5 spectrum at a cell temperature of 25°C.

4-terminal module with external dual-axis tracking. Power rating of CPV follows IEC 62670-3 standard, front power rating of flat plate PV based on IEC 60904-3, -5, -7, -10 and 60891 with modified current translation approach; rear power rating of flat plate PV based on IEC TS 60904-1-2 and 60891.

[p]Geometric concentration.

previously published[1] **are set in bold type**. In most cases, a literature reference is provided that describes either the result reported or a similar result (readers identifying improved references are welcome to submit to the lead author). Table 1 summarises the best-reported measurements for 'one-sun' (non-concentrator) single-junction cells and submodules.

Table 2 contains what might be described as 'notable exceptions' for 'one-sun' single-junction cells and submodules in the above category. While not conforming to the requirements to be recognised as a class record, the devices in Table 2 have notable characteristics that will be of interest to sections of the photovoltaic community, with entries based on their significance and timeliness. To encourage discrimination, the table is limited to nominally 15 entries with the present authors having voted for their preferences for inclusion. Readers who have suggestions for notable exceptions for inclusion into this or subsequent tables are welcome to contact any of the authors with full details. Suggestions conforming to the guidelines will be included on the voting list for a future issue.

Table 3 was first introduced in Version 49 of these tables and summarises the growing number of cell and submodule results involving high efficiency, one-sun multiple-junction devices (previously reported in Table 1). Table 4 shows the best results for one-sun modules, both single- and multiple-junction, while Table 5 shows the best results for concentrator cells and concentrator

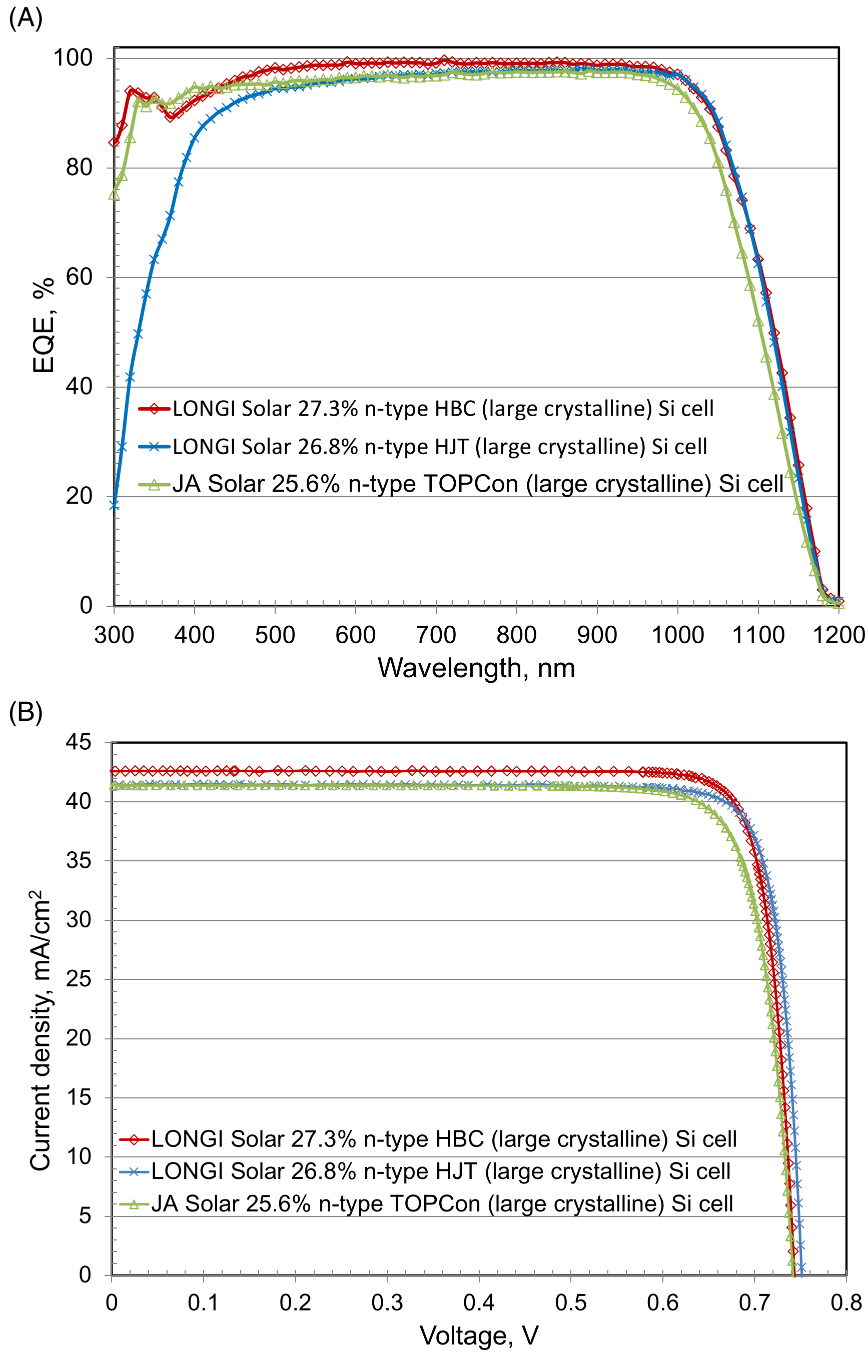

FIGURE 1 (A) External quantum efficiency (EQE) for the new silicon cell results reported in this issue (absolute values). (B) Corresponding current density–voltage (JV) curves.

modules. A small number of 'notable exceptions' are also included in Tables 3 to 5.

2 | NEW RESULTS

Nineteen new results are reported in the present version of these tables. The first is the very first entry reported in Table 1 ('one-sun cells and submodules'). An efficiency of 27.3% is reported for a large-area (243 cm^2) n-type silicon heterojunction interdigitated-back-contact (HBC) cell fabricated by LONGi Solar[4] and measured by the Institute für Solarenergieforschung (ISFH). The cell, establishing a new outright record for silicon, has both polarity contacts on the rear surface restricting loss by the absence of contacts on the front illuminated surface. An all-laser patterning process was used for the more complex rear surface patterning required for such devices.

The second new result is 13.45% efficiency for a 1-cm^2 $Cu_2ZnSn\text{-}S_ySe_{4\text{-}y}$ (CZTSSe) cell fabricated by the Institute of Physics, Chinese Academy of Sciences (IoP/CAS)[13] and measured by the Chinese National Photovoltaic Industry Measurement and Testing Center (NPVM). For similar CZTSSe material, an efficiency of 10.1% is reported for a 10.5-cm^2, six-cell minimodule fabricated by the Nanjing University of Posts and Telecommunications (NJUPT)[14] and measured by the US National Renewable Energy Laboratory (NREL). Another new result is 22.6% efficiency for a small area (20 cm^2) lead halide perovskite minimodule consisting of eight cells connected in series, with the minimodule fabricated by Singfilm Solar[19] and measured by NPVM.

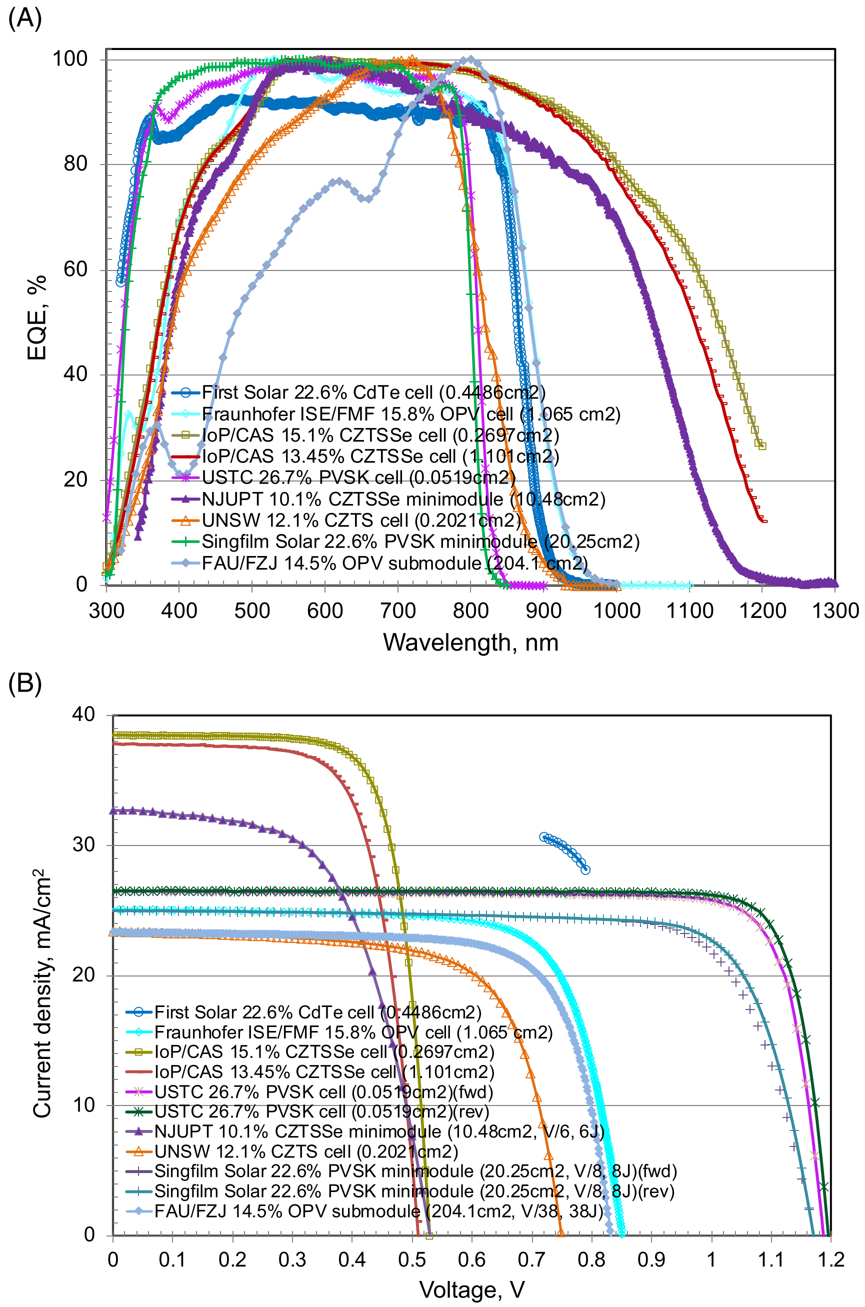

FIGURE 2 (A) External quantum efficiency (EQE) for new thin-film cell, minimodule and submodule results reported in this issue (some curves are normalised). (B) Corresponding current density–voltage (JV) curves.

The final new results in Table 1 involve two new organic cell and submodule results. The first is 15.8% efficiency for a 1-cm^2 organic cell[22] fabricated by the Fraunhofer Institute for Solar Energy Systems (FhG-ISE) and the Freiburg Materials Research Center (FMF) at the Albert-Ludwig University of Freiburg and measured at FhG-ISE. The second is a new record of 14.5% for a 204-cm^2 organic submodule[24] consisting of 38-serially connected cells, fabricated by Friedrich-Alexander-Universität, Erlangen-Nürnberg and Forschungszentrum Jülich GmbH (FAU/FZJ) and again measured by FhG-ISE.

Six new results are reported in Table 2 (one-sun 'notable exceptions'). The first is an increase in efficiency to 25.6% for a very large area (330 cm^2, the largest in these tables), silicon n-type TOPCon (tunnel oxide passivated contact) cell[34] fabricated by JASolar and measured by ISFH. The second is the movement of the result for the 26.8% efficient, large-area n-type silicon cell fabricated by LONGi Solar in 2022 from Table 1 to Table 2, notable since the most efficient, 'front-and-back' contacted silicon heterojunction (HJT) solar cell.

The next three results involve small area (<1 cm^2) chalcogenide thin-film solar cells. The first is an increase in efficiency to 22.6% for a small area (0.45 cm^2) CdTe-based cell fabricated by First Solar[39] and measured by NREL, improving on the 22.4% result first reported in the previous version of these tables.[1] The second new result is a similar efficiency increase to 15.1% for a small area (0.27 cm^2) CZTSSe cell fabricated by IoP/CAS[13] and measured by NPVM, improving on the 14.9% earlier result reported by IoP/CAS.[1] It is interesting to note that it took nearly 14 years for CZTSSe cell efficiency to improve from 10% to 15%, very similar to the time for the same transition for CIGS ($CuIn_yGa_{1-y}Se_2$) cells, now at 23.6% efficiency, while Pb-halide perovskite cells took only 18 months. Another new result is for a nominally pure-sulphide CZTS solar cell with efficiency increased to 12.1% for a small-area (0.2 cm^2) cell fabricated by the University of New South

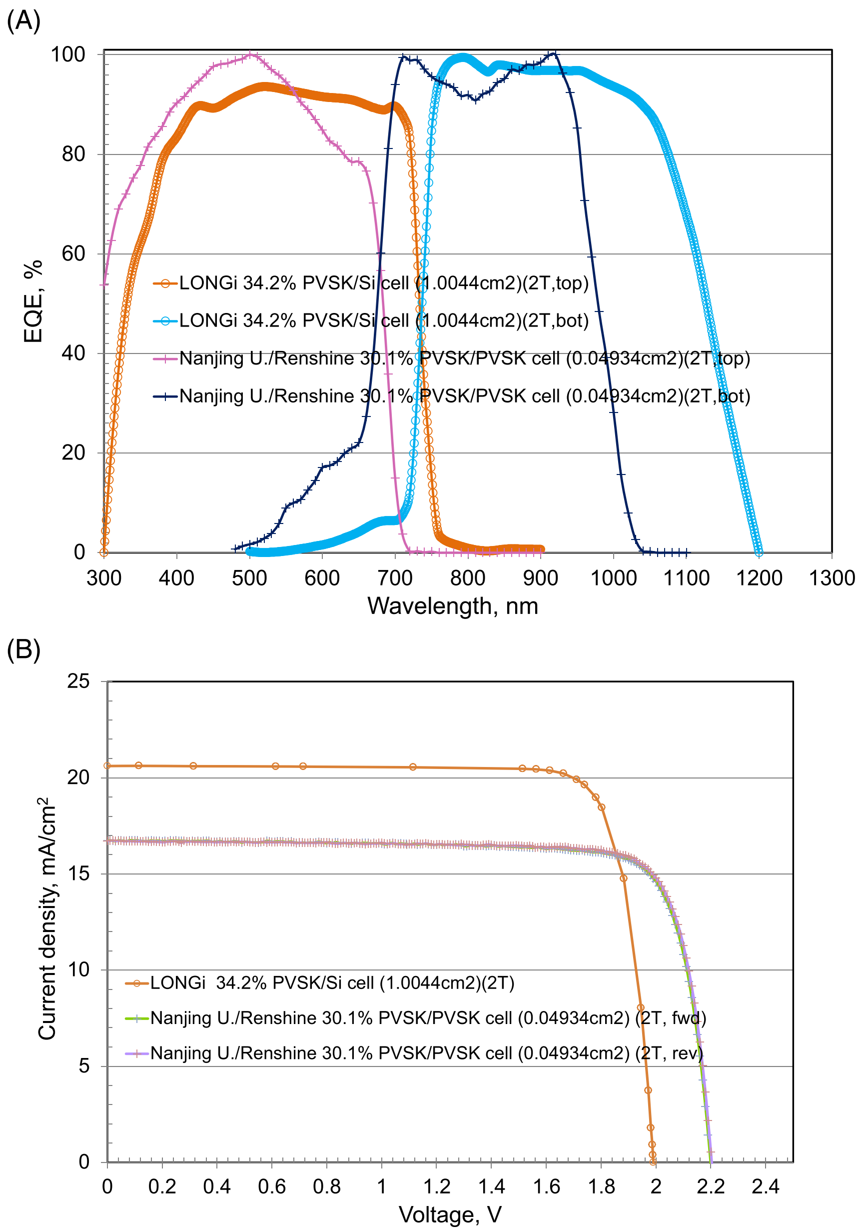

FIGURE 3 (A) External quantum efficiency (EQE) for new 2-terminal double-junction perovskite/Si and perovskite/perovskite multijunction cell results reported in this issue (results are normalised). (B) Corresponding current density–voltage (JV) curves.

Wales (UNSW), Sydney and again measured at NPVM. Since various alloying agents can reduce the bandgap (E_g) of this material increasing efficiency, future entries will be restricted to E_g > 1.5 eV, as determined from the maximum slope of the EQE curve. The final new result in Table 2 is an improvement to 26.7% efficiency for a very small area of 0.05-cm^2 Pb-halide perovskite solar cell fabricated by the University of Science and Technology China (USTC)[41] and measured by NPVM. For these last four results, cell area is too small for classification as an outright record, with solar cell efficiency targets in governmental research programs generally specified in terms of a cell area of 1 cm^2 or larger.[89–91]

There are two new results reported in Table 3 describing results for one-sun, multijunction devices—both involving perovskites in tandem cells. An efficiency of 34.2% is reported for a 1-cm^2, 2-terminal, silicon/perovskite tandem cell fabricated by LONGi Central R&D Institute and measured at the European Solar Test Installation (ESTI) at the European Commission's Joint Research Centre, Ispra, beating out LONGi's earlier 33.9% result. The second is an efficiency of 30.1% for a very small area 0.05-cm^2, 2-terminal, perovskite/perovskite tandem cell fabricated by Nanjing University and Renshine Solar (Suzhou) Co. Ltd and measured by the Japan Electrical Safety and Environment Technology Laboratories (JET).

There are five new results reported in Table 4 (one-sun modules) involving a range of technologies. The first is a new efficiency level of 24.9% reported for a 1.8-m^2 silicon module[60] fabricated by Maxeon Solar Technologies and measured by NREL. Maxeon is one of the

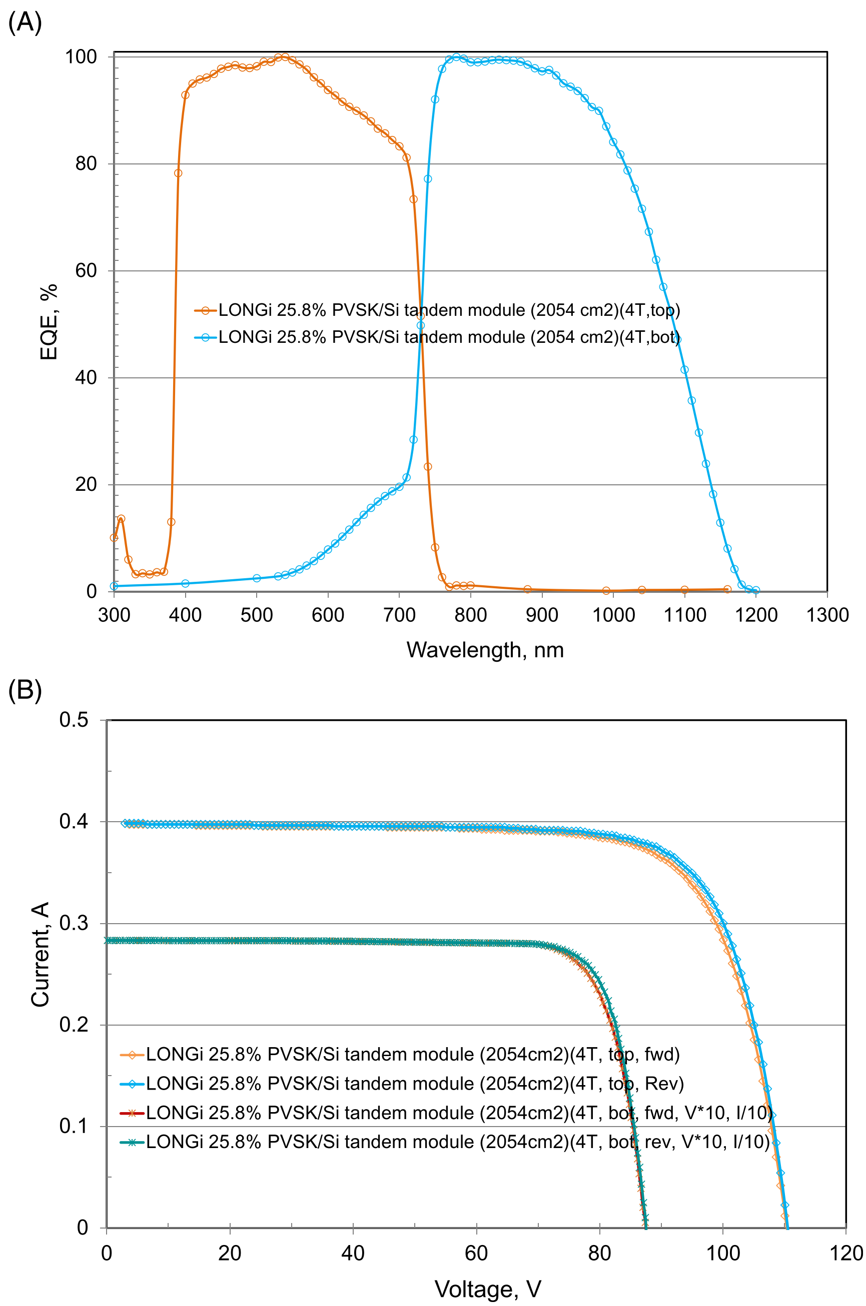

FIGURE 4 (A) External quantum efficiency (EQE) for the new 4-terminal perovskite/silicon tandem module result reported in this issue. (B) Corresponding current density–voltage (JV) curves.

leading proponents of the interdigitated-back-contact (IBC) cell. The second result is an improvement to 19.9% efficiency for a 2.4-m^2 CdTe-based thin-film module[63] fabricated by First Solar and also measured by NREL. The third is improvement to 19.2% efficiency for a smaller 1027-cm^2 perovskite thin-film module[64] fabricated by SolaEon and again measured by NREL.

The final 2 results in Table 4 also involve perovskites. The first of these falls in the multijunction module category efficiency where an efficiency of 25.8% is reported for a 2054-cm^2, 4-terminal silicon/perovskite tandem module fabricated by LONGi Green Energy Technologies and measured by FhG-ISE. The top perovskite cells contribute 15.9% absolute to the final 25.8% result with the bottom silicon cells contributing 9.9%. The final new result in Table 5 falls in the module 'notable exception' category with 15.0% total area efficiency reported for a large area (0.8 m^2) perovskite module[71] fabricated by Microquanta Semiconductor and again measured by FhG-ISE. This is a notable result since it represents the highest total area efficiency received for the tables for a perovskite module of this commercially relevant size.

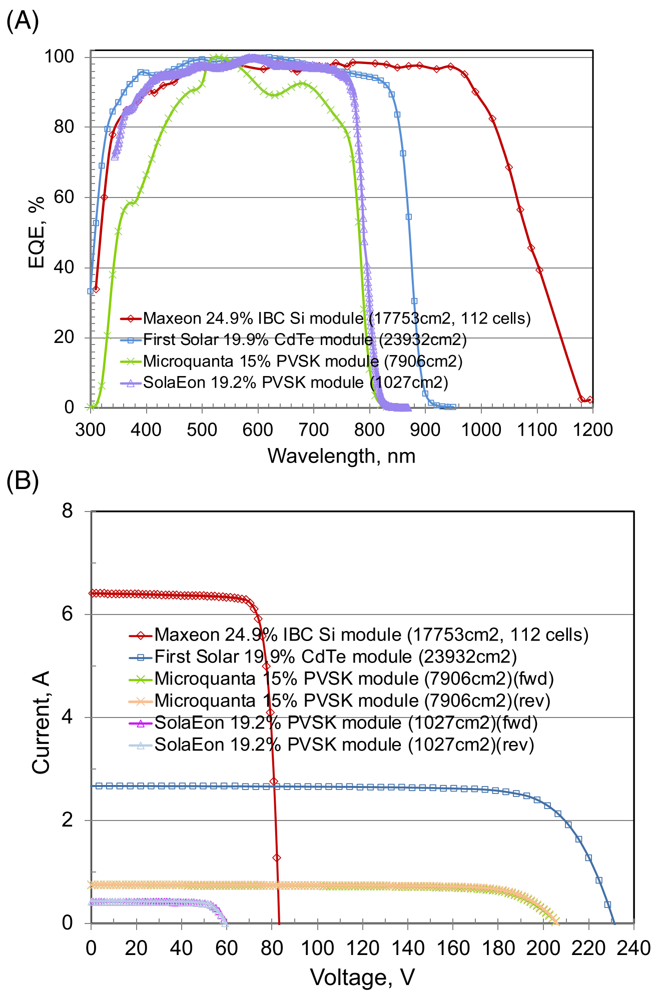

FIGURE 5 (A) External quantum efficiency (EQE) for the other new module results reported in this issue (some results are normalised). (B) Corresponding current density–voltage (JV) curves for these modules.

The EQE spectra for the new silicon cells reported in the present issue of these tables are shown in Figure 1A, with Figure 1B showing the current density–voltage (JV) curves for the same devices. Figure 2A,B shows the corresponding EQE and JV curves for several of the new thin-film cell and minimodule results. Figure 3A,B shows these for the new 2-terminal double-junction perovskite/Si and perovskite/perovskite multijunction cell results, while Figure 4A,B shows these for the new 4-terminal perovskite/Si tandem module result. Finally, Figure 5A,B shows EQE and JV curves for other new module results.

3 | DISCLAIMER

While the information provided in the tables is provided in good faith, the authors, editors and publishers cannot accept direct responsibility for any errors or omissions.

ACKNOWLEDGEMENTS

The Australian Centre for Advanced Photovoltaics commenced operation in February 2013 with support from the Australian Government through the Australian Renewable Energy Agency (ARENA). The Australian Government does not accept responsibility for the views, information or advice expressed herein. The work at NREL was supported by the U.S. Department of Energy under Contract No. DE-AC36-08-GO28308 with the National Renewable Energy Laboratory. The work at AIST was supported in part by the Japanese New Energy and Industrial Technology Development Organisation (NEDO) under the Ministry of Economy, Trade and Industry (METI). Open access publishing facilitated by University of New South Wales, as part of the Wiley - University of New South Wales agreement via the Council of Australian University Librarians.

DATA AVAILABILITY STATEMENT

The data that support the findings of this study are available from the corresponding author upon reasonable request.

ORCID

Martin A. Green https://orcid.org/0000-0002-8860-396X
Masahiro Yoshita https://orcid.org/0000-0003-1924-1288
Michael Rauer https://orcid.org/0000-0002-4150-6150

REFERENCES

1. Green MA, Dunlop ED, Yoshita M, Kopidakis N, Siefer G, Hao XJ. Solar cell efficiency tables (Version 63). *Progr Photovoltaics: Res Applic*. 2023;32(1):3-13. doi:10.1002/pip.3750
2. Green MA, Dunlop ED, Siefer G, Yoshita M, Kopidakis N, Hao XJ. Solar cell efficiency tables (Version 61). *Progr Photovoltaics: Res Applic*. 2022;31(1):3-16. doi:10.1002/pip.3646
3. Green MA, Dunlop ED, Hohl-Ebinger J, et al. Solar cell efficiency tables (Version 60). *Progr Photovoltaics: Res Applic*. 2022;30(7):687-701. doi:10.1002/pip.3595
4. https://www.longi.com/en/news/longi-hi-mo9-bc-world-record/
5. Moslehi MM, Kapur P, Kramer J, et al. World-record 20.6% efficiency 156 mm x 156 mm full-square solar cells using low-cost kerfless

ultrathin epitaxial silicon & porous silicon lift-off technology for industry-leading high-performance smart PV modules. In: *PV Asia Pacific Conference (APVIA/PVAP)*; 2012.
6. Keevers MJ, Young TL, Schubert U, Green MA. 10% efficient CSG minimodules. In: *22nd European Photovoltaic Solar Energy Conference*; 2007.
7. Kayes BM, Nie H, Twist R, et al. 27.6% conversion efficiency, a new record for single-junction solar cells under 1 sun illumination. In: *Proceedings of the 37th IEEE Photovoltaic Specialists Conference*; 2011.
8. Venkatasubramanian R, O'Quinn BC, Hills JS, et al. 18.2% (AM1.5) efficient GaAs solar cell on optical-grade polycrystalline Ge substrate. In: *Conference Record, 25th IEEE Photovoltaic Specialists Conference*; 1997:31-36.
9. Wanlass M. *Systems and Methods for Advanced Ultra-High-Performance InP Solar Cells*. US Patent 9,590,131 B2,2017.
10. Nakamura M, Yamaguchi K, Kimoto Y, Yasaki Y, Kato T, Sugimoto H. Cd-free Cu (In,Ga)(Se,S)2 thin-film solar cell with a new world record efficacy of 23.35%. In: *46th IEEE PVSC*. Vol.9, 6; 2019 (see also http://www.solar-frontier.com/eng/news/2019/0117_press.html): 1863-1867. doi:10.1109/JPHOTOV.2019.2937218
11. Diermann R. *Avancis claims 19.64% efficiency for CIGS module*. PV Magazine International; 2021. (https://www.pv-magazine.com/2021/03/04/avancis-claims-19-64-efficiency-for-cigs-module/)
12. *First Solar Press Release, First Solar Builds the Highest Efficiency Thin Film PV Cell on Record, 5* 2014.
13. Zhou J, Xu X, Wu H, et al. Control of the phase evolution of kesterite by tuning of the selenium partial pressure for solar cells with 13.8% certified efficiency. *Nat Energy*. 2023;8(5):526-535. doi:10.1038/s41560-023-01251-6
14. Gong Y, Zhang Y, Zhu Q, et al. Identifying the origin of the V_{oc} deficit of kesterite solar cells from the two grain growth mechanisms induced by Sn^{2+} and Sn^{4+} precursors in DMSO solution. *Energ Environ Sci*. 2021;14(4):2369-2380. doi:10.1039/D0EE03702H
15. Yan C, Huang J, Sun K, et al. $Cu_2ZnSn\ S_4$ solar cells with over 10% power conversion efficiency enabled by heterojunction heat treatment. *Nat Energy*. 2018;3(9):764-772. doi:10.1038/s41560-018-0206-0
16. Matsui T, Bidiville A, Sai H, et al. High-efficiency amorphous silicon solar cells: impact of deposition rate on metastability. *Appl Phys Lett*. 2015;106(5):053901. doi:10.1063/1.4907001
17. Sai H, Matsui T, Kumagai H, Matsubara K. Thin-film microcrystalline silicon solar cells: 11.9% efficiency and beyond. *Appl Phys Express*. 2018;11(2):022301. doi:10.7567/APEX.11.022301
18. Chen W, Zhu Y, Xiu J, et al. Monolithic perovskite/organic tandem solar cells with 23.6% efficiency enabled by reduced voltage losses and optimized interconnecting layer. *Nat Energy*. 2022;7(3):229-237. doi:10.1038/s41560-021-00966-8
19. Li J, Liang H, Xiao C, et al. Enhancing the efficiency and longevity of inverted perovskite solar cells with antimony-doped tin oxides. *Nat Energy*. 2024;9(3):308-315. doi:10.1038/s41560-023-01442-1
20. Han L, Fukui A, Chiba Y, et al. Integrated dye-sensitized solar cell module with conversion efficiency of 8.2%. *Appl Phys Lett*. 2009;94(1):013305. doi:10.1063/1.3054160
21. Komiya R, Fukui A, Murofushi N, Koide N, Yamanaka R, Katayama H. Improvement of the conversion efficiency of a monolithic type dye-sensitized solar cell module. In: *Technical Digest, 21st International Photovoltaic Science and Engineering Conference, Fukuoka*; 2011. 2C-5O-08.
22. Faisst J, Jiang E, Bogati S, et al. Organic solar cell with an active area > 1 cm2 achieving 15.8% certified efficiency using optimized VIS-NIR anti-reflection coating. *Sol RRL*. 2023;7(24):2300663. doi:10.1002/solr.202300663
23. https://www.pv-magazine.com/2021/03/17/organic-pv-module-with-12-36-efficiency/
24. https://www.pv-magazine.com/2024/03/08/large-area-organic-pv-module-achieves-world-record-efficiency-of-14-5/
25. Boyd CC, Cheacharoen R, Leijtens T, McGehee MD. Understanding degradation mechanisms and improving stability of perovskite photovoltaics. *Chem Rev*. 2019;119(5):3418-3451. doi:10.1021/acs.chemrev.8b00336
26. Yang Y, You J. Make perovskite solar cells stable. *Nature*. 2017;544(7649):155-156. doi:10.1038/544155a
27. Krašovec UO, Bokalič M, Topič M. Ageing of DSSC studied by electroluminescence and transmission imaging. *Solar Energy Mater Solar Cells*. 2013;117:67-72. doi:10.1016/j.solmat.2013.05.029
28. Tanenbaum DM, Hermenau M, Voroshazi E, et al. The ISOS-3 interlaboratory collaboration focused on the stability of a variety of organic photovoltaic devices. *RSC Adv*. 2012;2(3):882-893. doi:10.1039/C1RA00686J
29. Krebs FC (Ed). *Stability and Degradation of Organic and Polymer Solar Cells*. Wiley; 2012; Jorgensen M, Norrman K, Gevorgyan SA, Tromholt T, Andreasen B, Krebs FC. Stability of polymer solar cells. *Adv Mater*. 2012;24(5):580-612. doi:10.1002/adma.201104187.
30. Green MA. The passivated emitter and rear cell (PERC): from conception to mass production. *Solar Energy Mater Solar Cells*. 2015;143:190-197. doi:10.1016/j.solmat.2015.06.055
31. Richter A, Benick J, Feldmann F, Fell A, Hermle M, Glunz SW. n-Type Si solar cells with passivating electron contact: identifying sources for efficiency limitations by wafer thickness and resistivity variation. *Solar Energy Mater Solar Cells*. 2017;173:96-105. doi:10.1016/j.solmat.2017.05.042
32. Haase F, Klamt C, Schäfer S, et al. Laser contact openings for local poly-Si-metal contacts enabling 26.1%-efficient POLO-IBC solar cells. *Solar Energy Mater Solar Cells*. 2018;186:184-193. doi:10.1016/j.solmat.2018.06.020
33. Wang Q. Status of crystalline silicon PERC solar cells. In: *NIST/UL Workshop on Photovoltaic Materials Durability, Gaithersburg, MD USA*; 2019.
34. https://www.jasolar.com/index.php?m=content&c=index&a=lists&catid=464
35. Lin H, Yang M, Ru X, et al. Silicon heterojunction solar cells with up to 26.81% efficiency achieved by electrically optimized nanocrystalline-silicon hole contact layers. *Nat Energy*. 2023;8:789-799.
36. *LONGi Achieves New World Record for p-Type Solar Cell Efficiency*. Press Release:2022. https://www.longi.com/en/news/p-type-hjt-record/
37. NREL, *Private Communication*, 2019.
38. Keller K, Kiselman K, Donzel-Gargand O, et al. High-concentration silver alloying and steep back-contact gallium grading enabling copper indium gallium selenide solar cell with 23.6% efficiency. *Nat Energy*. 2024;9:467-478.
39. First Solar Press Release. *First Solar Achieves Yet Another Cell Conversion Efficiency World Record, 24* 2016.
40. Cui X, Sun K, Huang J, et al. Cd-Free Cu2ZnSnS4 solar cell with an efficiency greater than 10% enabled by Al2O3 passivation layer. *Energ Environ Sci*. 2019;12(9):2751-2764. doi:10.1039/C9EE01726G
41. http://en.ustc.edu.cn/info/1007/4676.htm
42. Zhu L, Ming Z, Xu J, et al. Single-junction organic solar cells with over 19% efficiency enabled by a refined double-fibril network morphology. *Nat Mater*. 2022;21(6):1-8. doi:10.1038/s41563-022-01244-y
43. Ren Y, Zhang D, Suo J, et al. Hydroxamic acid pre-adsorption raises the efficiency of cosensitized solar cells. *Nature*. 2023;613(7942):60-65. doi:10.1038/s41586-022-05460-z
44. Sasaki K, Agui T, Nakaido K, Takahashi N, Onitsuka R, Takamoto T. *Proceedings, 9th International Conference on Concentrating Photovoltaics Systems*, 2013.
45. Schygulla P, Müller R, Höhn O, et al. Wafer-bonded two-terminal III-V//Si triple-junction solar cell with power conversion efficiency of

36.1% at AM1.5g. In: *Presented at the 40th EU PVSEC*; 2023:Paper 2DO.9 (submitted to *Prog.Photovolt. Res. Appl.)*. doi:10.1002/pip.3769
46. Essig S, Allebé C, Remo T, et al. Raising the one-sun conversion efficiency of III–V/Si solar cells to 32.8% for two junctions and 35.9% for three junctions. *Nat Energy*. 2017;2:17144. doi:10.1038/nenergy.2017.144
47. Feifel M, Lackner D, Schön J, et al. Epitaxial GaInP/GaAs/Si triple-junction solar cell with 25.9% AM1.5g efficiency enabled by transparent metamorphic $Al_xGa_{1-x}As_yP_{1-y}$ step-graded buffer structures. *Sol RRL*. 2021;5(5):2000763. doi:10.1002/solr.202000763
48. Grassman TJ, Chmielewski DJ, Carnevale SD, Carlin JA, Ringel SA. $GaAs_{0.75}\ P_{0.25}$/Si dual-junction solar cells grown by MBE and MOCVD. *IEEE J. Photovoltaics*. 2016;6:326-331.
49. Green MA, Keevers MJ, Concha Ramon B, et al. Improvements in sunlight to electricity conversion efficiency: above 40% for direct sunlight and over 30% for global. In: *European Photovoltaic Solar Energy Conference 2015*; 2015:Paper 1AP.1.2.
50. https://www.oxfordpv.com/oxford-pv-story
51. Jošt M, Köhnen E, Al-Ashouri A, et al. Perovskite/CIGS tandem solar cells: from certified 24.2% toward 30% and beyond. *ACS Energy Lett*. 2022;7(4):1298-1307. doi:10.1021/acsenergylett.2c00274
52. Lin R, Xu J, Wei MY, et al. All-perovskite tandem solar cells with improved grain surface passivation. *Nature*. 2022;603(7899):73-78. doi:10.1038/s41586-021-04372-8
53. Xiao K, Lin YH, Zhang M, et al. Scalable processing for realizing 21.7%-efficient all-perovskite tandem solar modules. *Science*. 2022;376(6594):762-767. doi:10.1126/science.abn7696
54. Sai H, Matsui T, Koida T, Matsubara K. Stabilized 14.0%-efficient triple-junction thin-film silicon solar cell. *Appl Phys Lett*. 2016;109(18):183506. doi:10.1063/1.49669996
55. Matsui T, Maejima K, Bidiville A, et al. High-efficiency thin-film silicon solar cells realized by integrating stable a-Si:H absorbers into improved device design. *Jpn J Appl Phys*. 2015;54:08KB10. doi:10.7567/JJAP.54.08KB10
56. Accessed October 28, 2018. http://mldevices.com/index.php/news/
57. Geisz JF, Steiner MA, Jain N, et al. Building a six-junction inverted metamorphic concentrator solar cell. *IEEE J Photovoltaics*. 2018;8(2):626-632. doi:10.1109/JPHOTOV.2017.2778567
58. Makita K, Kamikawa Y, Mizuno H, et al. III-V//$Cu_xIn_{1-y}Ga_ySe_2$ multijunction solar cells with 27.2% efficiency fabricated using modified smart stack technology with Pd nanoparticle array and adhesive material. *Prog Photovolt Res Appl*. 2021;29(8):887-898. doi:10.1002/pip.3398
59. Chen W, Zhu YD, Xiu JW, et al. Monolithic perovskite/organic tandem solar cells with 23.6% efficiency enabled by reduced voltage losses and optimized interconnecting layer. *Nature Energy*. 2022;7:229-237. https://doi.org/10.1038/s41560-021-00966-8
60. https://mediaroom.maxeon.com/2024-03-21-Maxeon-Sets-Another-Solar-Panel-Efficiency-Benchmark-and-Achieves-Leading-Reliability-Certification
61. Mattos LS, Scully SR, Syfu M, et al. New module efficiency record: 23.5% under 1-sun illumination using thin-film single-junction GaAs solar cells. In: *Proceedings of the 38th IEEE Photovoltaic Specialists Conference*; 2012.
62. Sugimoto H. High efficiency and large volume production of CIS-based modules. In: *40th IEEE Photovoltaic Specialists Conference*; 2014.
63. Accessed October 28, 2019.http://www.firstsolar.com/en-AU/-/media/First-Solar/Technical-Documents/Series-6-Datasheets/Series-6-Datasheet.ashx
64. https://taiyangnews.info/solaeon-technology-announces-world-record-for-perovskite-modules/
65. Hosoya M, Oooka H, Nakao H, et al. Organic thin film photovoltaic modules. In: *Proceedings of the 93rd Annual Meeting of the Chemical Society of Japan*; 2013:21-37.
66. *Sharp Achieves World's Highest*[*1] *Conversion Efficiency of 32.65%*[*2] *in a Lightweight, Flexible, Practically Sized Solar Module*. Press Release: 2022. https://global.sharp/corporate/news/220606-a.html
67. Wright M, Vicari Stefani B, Jones TW, et al. Design considerations for the bottom cell in perovskite/silicon tandems: a terawatt scalability perspective. *Energ Environ Sci*. 2023;16(10):4164-4190. doi:10.1039/D3EE00952A
68. Cashmore JS, Apolloni M, Braga A, et al. Improved conversion efficiencies of thin-film silicon tandem (MICROMORPH™) photovoltaic modules. *Solar Energy Mater Solar Cells*. 2016;144:84-95. doi:10.1016/j.solmat.2015.08.022
69. Bheemreddy V, Liu BJJ, Wills A, Murcia CP. Life prediction model development for flexible photovoltaic modules using accelerated damp heat testing. In: *IEEE 7th World Conf on Photovoltaic Energy Conversion (WCPEC)*; 2018:1249-1251.
70. Takamoto T, Juso H, Ueda K, et al. IMM triple-junction solar cells and modules optimized for space and terrestrial conditions. *Proceedings of the 44th IEEE Photovoltaic Specialist Conference (PVSC)*. 2017. doi:10.1109/PVSC.2017.8366097
71. Higuchi H, Negami T. Largest highly efficient 203 x 203 mm^2 $CH_3NH_3PbI_3$ perovskite solar modules. *Jpn J Appl Phys*. 2018;57(8S3):08RE11. doi:10.7567/JJAP.57.08RE11
72. Slade A, Garboushian V. 27.6% efficient silicon concentrator cell for mass production. In: *Technical Digest, 15th International Photovoltaic Science and Engineering Conference*; 2005:701.
73. Ward JS, Ramanathan K, Hasoon FS, et al. A 21.5% efficient Cu (In,Ga)Se2 thin-film concentrator solar cell. *Progr Photovoltaics: Res Applic*. 2002;10(1):41-46. doi:10.1002/pip.424
74. Dimroth F, Tibbits TND, Niemeyer M, et al. Four-junction wafer-bonded concentrator solar cells. *IEEE J Photovoltaics*. 2016;6(1):343-349. doi:10.1109/JPHOTOV.2015.2501729
75. NREL. *Press Release NR-4514, 16* 2014.
76. *Press Release**, *Sharp Corporation*, 2012 (accessed at http://sharp-world.com/corporate/news/120531.html on 5 June 2013).
77. Jain N, Schulte KL, Geisz JF, et al. High-efficiency inverted metamorphic 1.7/1.1 eV GaInAsP/GaInAs dual-junction solar cells. *Appl Phys Lett*. 2018;112(5):053905. doi:10.1063/1.5008517
78. Steiner M, Siefer G, Schmidt T, Wiesenfarth M, Dimroth F, Bett AW. 43% sunlight to electricity conversion efficiency using CPV. *IEEE J Photovoltaics*. 2016;6(4):1020-1024. doi:10.1109/JPHOTOV.2016.2551460
79. Green MA, Keevers MJ, Thomas I, Lasich JB, Emery K, King RR. 40% efficient sunlight to electricity conversion. *Progr Photovoltaics: Res Applic*. 2015;23(6):685-691. doi:10.1002/pip.2612
80. Chiang CJ, Richards EH. A 20% efficient photovoltaic concentrator module. In: *Conf. Record, 21st IEEE Photovoltaic Specialists Conference, Kissimimee*; 1990:861-863.
81. Accessed October 23, 2013. http://amonix.com/pressreleases/amonix-achieves-world-record-359-module-efficiency-rating-nrel-4
82. van Riesen S, Neubauer M, Boos A, et al. New module design with 4-junction solar cells for high efficiencies. In: *Proceedings of the 11th Conference on Concentrator Photovoltaic Systems*; 2015.
83. Martínez JF, Steiner M, Wiesenfarth M, Siefer G, Glunz SW, Dimroth F. Power rating procedure of hybrid CPV/PV bifacial modules. *Prog Photovolt Res Appl*. 2021;29(6):614-629. doi:10.1002/pip.3410
84. Zhang F, Wenham SR, Green MA. Large area, concentrator buried contact solar cells. *IEEE Trans Electron Devices*. 1995;42(1):144-149. doi:10.1109/16.370024
85. Slooff LH, Bende EE, Burgers AR, et al. A luminescent solar concentrator with 7.1% power conversion efficiency. *Phys Stat Sol (RRL)*. 2008;2(6):257-259. doi:10.1002/pssr.200802186
86. Steiner M, Wiesenfarth M, Martínez JF, Siefer G, Dimroth F. Pushing energy yield with concentrating photovoltaics. *AIP Con Proc*. 2019;2149:060006. doi:10.1063/1.5124199
87. Müllejans H, Winter S, Green MA, Dunlop ED. *What Is the Correct Efficiency for Terrestrial Concentrator PV Devices? 38th European Photovoltaic Solar Energy Conference*, 2021.

88. Gueymard CA, Myers D, Emery K. Proposed reference irradiance spectra for solar energy systems testing. *Solar Energy*. 2002;73(6): 443-467. doi:10.1016/S0038-092X(03)00005-7
89. *Program Milestones and Decision Points for Single Junction Thin Films*. *Annual Progress Report* 1984. Photovoltaics, Solar Energy Research Institute, *Report* DOE/CE-0128; 1985:7.
90. Sakata I, Tanaka Y, Koizawa K, Japan's New National R&D Program for Photovoltaics. *Photovoltaic energy conversion, conference record of the* 2006. In: *IEEE 4th World Conference*. Vol.1; 2008:1-4.
91. Jäger-Waldau A (Ed). *PVNET: European Roadmap for PV R&D, EUR 21087 EN*. Vol. 451-452; 2004:448-454. doi:10.1016/j.tsf.2003.10.140

How to cite this article: Green MA, Dunlop ED, Yoshita M, et al. Solar cell efficiency tables (Version 64). *Prog Photovolt Res Appl*. 2024;32(7):425-441. doi:10.1002/pip.3831

APPENDIX A: CELL PROBING

In contrast to the electrical contacting of modules or reference solar cells, which usually have standardised plug connections, measuring the electrical properties of bare solar cells is much more challenging. As there are no specifications for the design of contacting schemes, various solutions can be found.

The determination of the current–voltage characteristics of a solar cell under illumination requires measuring current–voltage pairs that match, which means that current and voltage values must correspond to the same state of operation of the solar cell.

It is important to understand that during measurements in calibration laboratories, solar cells are not necessarily contacted in the same way as they are later connected in the module. Instead, measurement conditions must be chosen so that the results from different laboratories agree (within their respective measurement uncertainties), even if they use different solutions for contacting the bare cells.

Most solar cells with contacts on front and rear have busbars for electrical interconnection in the photovoltaic module made from these cells. The most widely used approach for a temporary non-destructive electrical contacting for measuring the current–voltage characteristics of such cells is to use contact bars equipped with spring-loaded pins.

As shown in Figure A1, parabolic voltage distributions $V(x)$ are formed between the pins used for current extraction. The further apart the current contacts and the lower the lateral conductivity of the busbar, the higher the amplitude ΔV of the voltage curves. Consequently, as Figure A1 also shows, the position of the voltage sensing pins in relation to the position of the pins used for current extraction has a significant impact on the fill factor of the measured current–voltage curve and thus on the reported energy conversion efficiency.

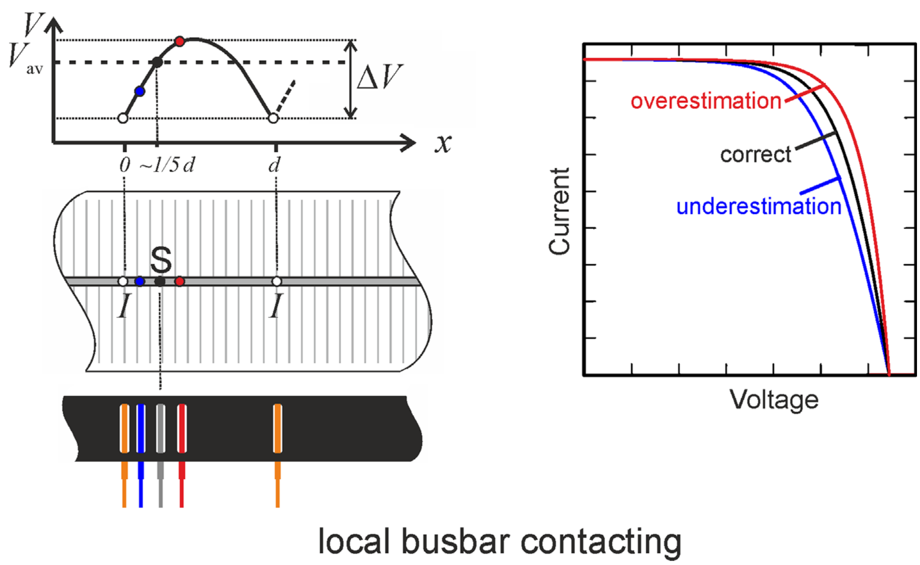

FIGURE A1 Local contacting of a homogenous busbar with contacting pins. Orange pins mark the positions of the current contacts on the busbar. To probe the average busbar potential, the sensing must be performed at ~1/5th of the distance of the two current pins (grey). A smaller distance (blue) results in an underestimation whereas a larger distance (red) results in an overestimation of the solar cell performance.

If probing the voltage close to the current pin (blue-coloured sensing position), one assigns low voltages to the current values, giving a small fill factor and thus an underrated energy conversion efficiency. Probing at a large distance (red-coloured sensing position), higher voltage values are assigned and consequently a high fill factor, and thus, an overrated efficiency is obtained. To find the correct position for the voltage sensing pin, we assume a sufficiently high overall lateral conductivity of the solar cell. The solar cell then operates at the average busbar potential V_{av} as a first approximation. Thus, to measure the correct voltage value corresponding to the extracted current, one must probe this average busbar potential using a smart sensing approach. For equally spaced current pins, the voltage probe must be placed at approximately 1/5th of the distance between two current contacts (grey-coloured sensing position).[A1,A2]

Voltage measurements at ~1/5th of the distance between two current pins are not the only way to probe the average busbar voltage—there are a variety of different contact schemes suitable for the smart sensing approach.[A1]

Triplets for example, as shown in Figure A2, have been used successfully in the past for calibration measurements.[A1,A3] They have the advantage that they are more robust against technically almost unavoidable variations in the contacting resistance[A1] occurring between the spring-loaded pin and the solar cell busbar. By calculating the average busbar potential resulting from the two parabolic distributions between the triplets and within a triplet, it can be shown analytically that the ideal distance d_1 between the triplets is equal to $\left(1+\sqrt{3}\right)/2 \approx 1.37$ the distance d_2 within one triplet.

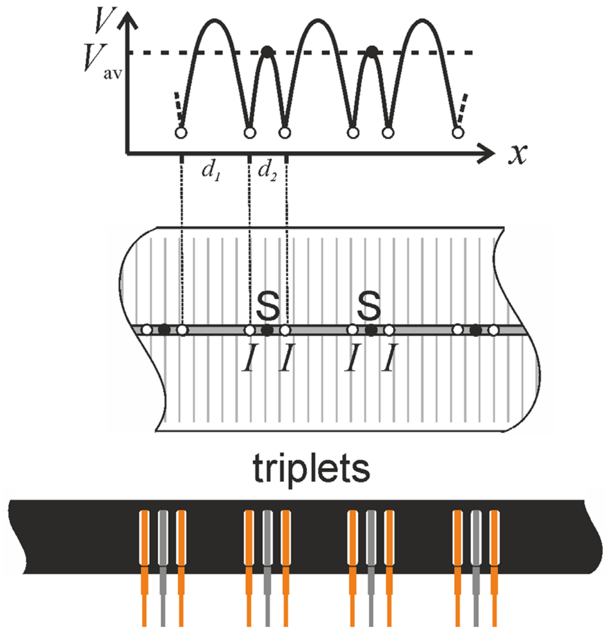

FIGURE A2 Local busbar contacting by means of current–voltage–current pin triplets. The spacing of the current probes is ideally ~1.37 wider between triplets (d_1) than within each triplet (d_2).

With decreasing width of the busbar down to values well below 100 μm, for structured layouts as well as dashed or non-homogenous busbars, the use of spring-loaded pins reaches its technical limits. Consequently, it becomes increasingly difficult to obtain reliable electrical contacts between the pins and the busbars. For such solar cells contacting schemes contacting the entire metal surface of the busbar homogeneously are favourable. The decisive advantage of such a full-busbar contacting is that no voltage distributions are formed along the busbar. As long as the solar cell itself is homogeneous, the voltage V_{BB} is constant over the entire busbar. As shown in Figure A3, the busbar voltage V_{BB} can either be measured with a narrow segment (a) or with an additional contact in parallel to the current contact (b). While the first approach requires a very narrow sense segment with the width *w*, the distance *t* between the parallel current and sense contacts in the second approach must be as small as possible to keep the overestimation of the busbar voltage and thus the overestimation of the solar cell energy conversion efficiency at a minimum.

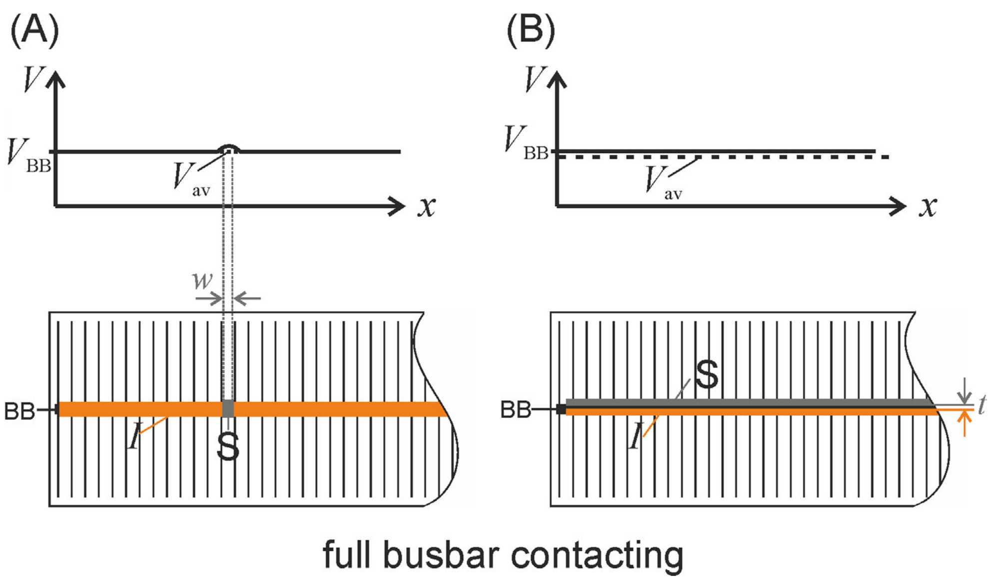

FIGURE A3 Full-busbar surface contacting: (A) voltage sensing with a very narrow sense segment on the busbar (BB) or (B) voltage sensing parallel to the current contact on or in the direct vicinity of the busbar.

A suitable method for checking the homogeneity of the respective contacting approach is to take an electroluminescence image. For meaningful images, the EL intensity should be captured at a current that corresponds to the current at the maximum power point (I_{MPP}).

Unfortunately, as already discussed with respect to Figure 1, there are many ways of misplacing the voltage sensing contact. Figure A4 shows two of them for contacting bars with equidistant current pins. One unfavourable contacting scheme as shown in Figure A4A follows from the replacement of a current contact by a voltage contact. In this case, the assigned voltage is overestimated by ΔV_{over}, and the fill factor is artificially increased and solar cell performance is overestimated. Even placing the voltage contact centred between equally spaced current pins as shown in Figure A4B results in an overestimation of the measured voltage and thus to an overestimation of the fill factor, even though the overestimation is less drastic.

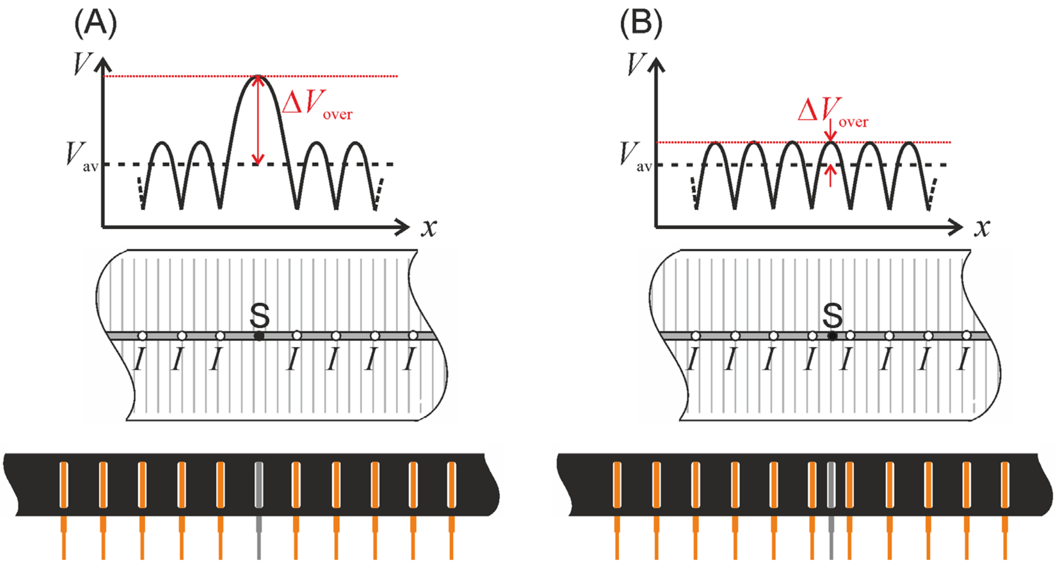

FIGURE A4 Two unfavourable contacting schemes for contacting bars with equidistant current pins: (A) replacement of a current pin by a voltage sensing pin, (B) additional voltage sensing pin centred between two current pins. Both approaches overestimate the average busbar voltage by ΔV_{over}. Consequently, the fill factor is overestimated and therefore also the attributed energy conversion efficiency.

In conclusion and as a design rule for contacting bars, it can be stated that for current multi-busbar solar cells with very thin and structured busbars, reliable contacting schemes contact the entire metal surface of the busbar. If this is not possible, it is advisable to use as many current pins as possible to keep the voltage amplitude of the parabolic voltage curve as small as possible. In addition, a smart sensing approach probing the average busbar voltage must be implemented. The sense pins should be distributed homogeneously over the solar cell surface. More sense pins are preferable, as they provide the average cell voltage more reliably for solar cells with an inhomogeneous performance.

REFERENCES (for Appendix A):

A1. Kruse CN, Wolf M, Schinke C, Hinken D, Brendel R, Bothe K. Impact of contacting geometries when measuring fill factors of solar cell current–voltage characteristics. IEEE Journal of Photovoltaics, 2017, 7, 3, pp. 747–754.

A2. Rauer M, Krieg A, Pfreundt A, Mittag M, Pingel S. The challenge of measuring busbarless solar cells and the impact on cell-to-module losses. Photovolt. Int. 2020, 45, pp. 8–18.

A3. Hohl-Ebinger J, Grote D, Hund B, Mette A, Warta W. Contacting bare solar cells for STC measurements. Proceedings of the 23rd European Photovoltaic Solar Energy Conference and Exhibition, Valencia, Spain, 2008, pp. 2012–2016.

APPENDIX B: DESIGNATED TEXT CENTRES

Designated test centres are listed in Version 61 and Version 62. One change from these earlier lists is that the contact for the Newport PV lab (MKS Instruments) has changed to:

Nagel, Garrett garrett.nagel@mksinst.com.